ORIGINAL ARTICLE

Thermal properties of 3D printed products from the most common polymers

Irina Bute[1] · Sergejs Tarasovs[1] · Sergejs Vidinejevs[1] · Laima Vevere[2] · Jevgenijs Sevcenko[1] · Andrey Aniskevich[1]

Abstract

This research focuses on four thermal characteristics of 3D products printed from the fourteen most common filaments. The softening temperature, coefficient of linear thermal expansion (CLTE), irreversible thermal strain, and thermal conductivity of the 3D printed samples at various measurement directions were evaluated, systematised, and analysed. Semi-crystalline and amorphous, electrically conductive and thermochromic polymer filaments were investigated. Four sets of samples were printed by the Ultimaker S5 3D printer. Printer settings provided the unidirectional orientation of all filament fibres in all specimens and uniform within any specimen's cross section to investigate the anisotropy of their properties. For investigation of the thermal characteristic of the 3D printed samples, thermomechanical analysis (TMA), differential scanning calorimetry (DSC) methods, and method for measurement of the thermal conductivity (Hot-Disk) were used. The penetration test showed that polyetherimide samples had the highest heat resistance, while the samples from polylactic acid (PLA) had the lowest one. The results of TMA demonstrated that the samples of polypropylene (PP), thermoplastic polyurethane (TPU), and Polyamide had the highest CLTE. In general, semi-crystalline polymers had a higher coefficient of thermal expansion than amorphous ones. During the TMA, almost all samples showed an irreversible thermal strain. PLA Red and Co-polyester showed significant shrinkage of 6–9% in the print direction and expansion in the build direction compared to other samples. Samples of PLA LAVA, acrylonitrile butadiene styrene, polycarbonate, PP, and TPU filaments demonstrated more stable thermal behaviour. The thermal conductivity analysis showed that almost all specimens had a certain degree of anisotropy. The highest thermal conductivity value was obtained for print direction for materials with pronounced anisotropic behaviour, except for polyamide samples. DSC study of post-printing relaxation of the structure of printed samples showed that rapidly cooled samples of semi-crystalline PLA material had a non-equilibrium structure with a low degree of crystallinity. Such structures changed with the time up to 400 h after printing, which also affected their stiffness and strength. The annealing of printed samples at temperatures of cold crystallisation allowed a significant increase in their crystallinity degree, thus approaching the upper limit of this degree for semi-crystalline PLA.

Keywords Thermoplastic · Anisotropy · Coefficient of linear thermal expansion · Thermal conductivity · Irreversible thermal strain

1 Introduction

Three-dimensional (3D) printing is one of the additive manufacturing (AM) techniques to create objects with the desired form by building layer-by-layer [1]. 3D printing has different techniques like selective laser sintering (SLS) material jetting, stereolithography (SLA), material extrusion (fused deposition modelling), binder jetting, etc., for different materials and areas [2, 3]. Fused deposition modelling (FDM) is one of the most widely used 3D printing techniques due to its ease of use, low cost, and environmental friendliness. FDM is increasingly used in product development, prototyping, and manufacturing processes in various industries, including automotive [4], architecture, medical appliances [5], and aerospace [6]. Filaments from commercially available thermoplastic materials like acrylonitrile butadiene styrene (ABS), polylactic acid (PLA),

✉ Irina Bute
  irina.bute@lu.lv

1 Institute for Mechanics of Materials, University of Latvia, Jelgavas St. 3, Riga 1004, Latvia

2 Latvian State Institute of Wood Chemistry, Dzerbenes St. 27, Riga 1006, Latvia

polycarbonate (PC), polyamide (PA), and polyetherketoneketone (PEKK), etc., are widely used for the FDM process [7]. Despite many advantages of this technology, there are several disadvantages: weak mechanical properties, layered construction, and poor surface quality.

Present technologies in AM are focused on improving the mechanical and electrical properties of 3D printed structures. But there is almost no literature on the experimental determination of the thermal properties of 3D printed products. The research data on thermal characteristics, which was published, are scattered. Some articles focus on the thermal properties of filaments only [8], while others focus on specific thermal characteristics [9]. The data on thermal properties are important because they show the formation of bonds between the filaments, and the quality of these bonds affects the mechanical [7] and electrical [9] properties.

Another aspect of the need to study thermal properties is the anisotropy of properties and the reduction of characteristics due to residual stress, which has often been observed in additively manufactured polymers. During the product's build-up, repeating the heating and cooling of the material residual stresses and strains cause [10]. Residual stress build-up is commonly seen in composite systems due to mismatches in coefficients of linear thermal expansion (CLTE). For instance, similar mismatches of CLTE can arise when a molten polymer is printed on top of a glassy polymer [11]. That is why thermal characteristics such as softening temperature, CLTE, and thermal conductivity play an essential role in the choice of material to manufacture a printed product.

The thermoplastic materials tend to shrink during the cooling process, resulting in a warp of the printed products [12]. Annealing of parts to relieve stresses sometimes led to irreversible thermal strain (ITS), which remained after cooling the parts to room temperature [13].

Inherent anisotropy of the properties of the parts produced by FDM technology was the subject of numerous works. A review of the anisotropic behaviour (mostly mechanical) in additively manufactured polymers and polymer composites was published in [14]. Due to the increasing popularity of the FDM 3D printing technique, more attention in recent years has been given to the investigation of the anisotropy of thermal properties.

Thermal properties of the printed parts became more important with the introduction of the filaments from modified polymers with highly conductive filler, where increased thermal conductivity compared to pure polymers can be obtained. Several works investigating the effect of the filler content and orientation on the thermal properties of printed polymer composites were published recently. Several works reported significant anisotropy in the thermal conductivity of the samples printed from modified polymers due to the filler orientation on the print direction [9, 15–18]. The influence of the fibre orientations on the mechanical and thermal conductivity properties of PP composites filled with short-CF was studied in [15]. The thermal conductivity of 3D printed continuous fibre polymer composites was evaluated in [16], and values up to 2.97 W/m·K were obtained. Anisotropy of the thermal properties of the printed highly oriented liquid crystalline polymer filled with boron nitride particles was investigated in [17]. Specific heat and anisotropic thermal conductivity at different temperatures of three polymers, ABS, polyphenylsulfone, and polyphenylene sulfide, filled with carbon fibres were measured in [18].

Another aspect of the published studies is the influence of the printing parameters on the thermal conductivity of the samples. The steady-state meter bar method was used to measure the anisotropic thermal conductivity of pure and modified PLA 3D printed samples [19]. It was found that the thermal conductivity of printed samples is influenced by contact resistance between printed filament rasters. The effects of the layer height, fill ratio, and line width on the thermal conductivity of the pure and modified PLA samples were studied in [20]. The effects of infill density, printing speed, layer height, and raster angles on the thermal conductivity of the PLA samples were investigated in [21]. The effect of thermal annealing was studied in [22] and the improvement of over 150% of thermal conductivity was obtained for ABS samples.

Characterisation of the anisotropic thermal properties of different polymers commonly used in FDM printers is very important for understanding the fundamental structure-properties relationships and predicting the thermal properties of the printed parts.

Since thermal properties are one of the essential factors in choosing a material to manufacture a 3D printed product, this work aimed to evaluate, systematise, and provide a comparative analysis of the main thermal characteristics of the most common thermoplastic materials. To achieve this purpose, the softening temperature of the material limiting the upper operating temperature, CLTE at various temperatures ranges, thermal conductivity, ITS, and post-printing relaxation of a structure of the tested materials at the various directions of the measurements should be evaluated, systematised, and analysed.

2 Materials

In this work, the Ultimaker S5 3D printer (Ultimaker B.V., The Netherlands) with a 0.4-mm-diameter nozzle was used to produce the specimens from filaments of 2.85-mm diameter, except PEKK and PEI samples. The nozzle and bed temperatures depend on the material and are given in Table 1. The print head speed was 20 mm/s. The layer thickness was set at 0.1 mm for most specimens, as seen in

Table 1 List of tested materials with a grade of supplier and print parameters

Material, Short name, grade (notation)	Supplier	Nozzle temperature, ℃	Bed temperature, ℃	Layer thickness, mm
Polylactic acid, PLA, Tough White 20,231 (PLA_TW)	Ultimaker	225	70	0.1
PLA Red	Devil Design	200	60	0.1
PLA Super Blue (PLA_SB)	Devil Design	200	60	0.1
PLA LAVA*, CY190415lyjzys2	Hello3d	200	60	0.1
PLA conductive**, CDP12805 Batch 171,201	Proto-pasta	200	60	0.1
Polyethylene terephthalate glycol, PET-G, White	Devil Design	235	85	0.1
Acrylonitrile butadiene styrene, ABS, White 1622	Ultimaker	240	85	0.1
Co-polyester, CPE, White UM-9703-A	Ultimaker	240	70	0.1
Polycarbonate PC, White 1642	Ultimaker	270	110	0.1
Polypropylene, PP, Natural	Ultimaker	225	70	0.1
Thermoplastic polyurethane, TPU95A, White 1755	Ultimaker	223	70	0.1
Polyamide PA, Nylon Transparent 1647	Ultimaker	245	70	0.1
Poly(ether ketone ketone) PEKK, Antero 800NA	Stratasys	395	180	0.25
Polyetherimide, PEI, ULTEM 9085 CG	Stratasys	385	180	0.25

*Thermochromic.

**Filled with carbon black.

Table 1. In all cases, the infill pattern was set to "Lines", fibre width ("Line width") was set to 0.35 mm, and infill density was set to 100%. Shell and top/bottom thickness settings were set to zero. These printer settings provided the unidirectional orientation of all filament fibres in all specimens and uniform within any specimen's cross section.

Four sets of samples were prepared for the evaluation of thermal properties. The first set of samples with sizes $7 \times 7 \times 3$ mm was cut from dog-bone samples and used to evaluate softening temperature using penetration measurements by thermomechanical analysis (TMA). The second and third sets of samples with sizes $10 \times 10 \times 10$ mm and $5 \times 5 \times 5$ mm (PEKK, PEI) were fabricated for evaluation of CLTE and ITS (Fig. 1). The PEKK and PEI samples were not included in the comparison because a different printer and different print settings were used for printing.

To determine the thermal conductivity of the FDM printed polymers, the fourth set of cubic samples with dimensions $25 \times 25 \times 25$ mm was printed. Two identical samples were printed for each investigated material (except for PLA SB due to lack of filament) with a layer height of 0.1 mm (0.25 mm for PEKK and PEI). All cube sides were polished in each sample allowing measuring properties in three mutually orthogonal directions (Fig. 1). The print and build directions marked as *X* and *Z*, respectively, for all printed samples, are illustrated in Fig. 2.

3 Methods

3.1 Thermomechanical analysis

Penetration measurements by TMA performed with Mettler-Toledo TMA/SDTA 841e were used to evaluate a sample's softening temperature or softening point. The penetration of a ball-point probe into the sample under an applied load of 1 N was measured as a function of temperature in the range of 30–130 ℃ (in some cases up to 240 ℃) with a heating rate of 2 °C/min.

The TMA curve shows the relative penetration depth of the probe concerning the initial sample thickness as a function of temperature (Fig. 3). At the beginning of heating, the curve is close to linear because of the thermal expansion of the sample. As the material softens and the probe continues to penetrate the sample, the curve in the graph decreases rapidly. The temperature of softening T_S was determined as the point of intersection of two tangent lines, as shown in Fig. 3. The error evaluation showed that the accuracy of determining T_S was approximately 1 ℃.

To examine CLTE and ITS, the printed samples were tested by TMA. The measurements were taken in three directions *X*, *Y*, and *Z* (Fig. 2). The samples were subjected to two heating/cooling cycles in the temperature range from 30 ℃ to approximately T_S with a heating rate of 1 ℃/min. The ITS values were obtained from the first

Fig. 1 Example of the investigated samples. Big cubic samples with dimensions 25×25×25 mm for determination of the thermal conductivity, and samples with sizes 10×10×10 mm for evaluation of CLTE and ITS
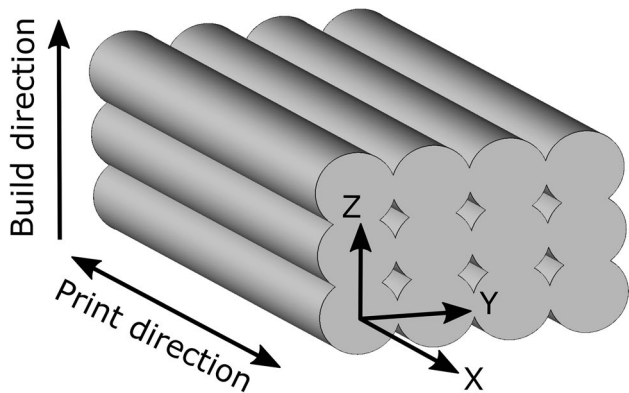
Fig. 2 Illustration of print and build directions of 3D printed samples
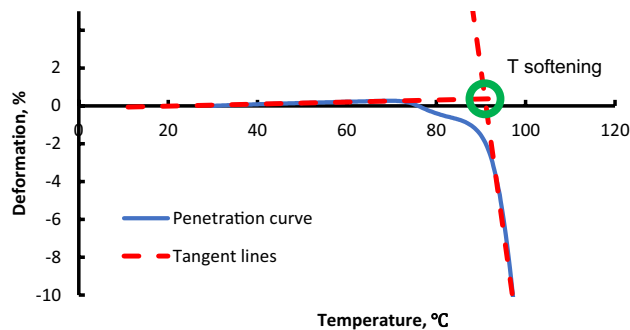
Fig. 3 Determination of softening temperature T_S for ABS sample by a TMA penetration test

heating/cooling cycle using the obtained dependencies of deformation on temperature (see Fig. 4). CLTE values were determined for various temperature ranges on the second heating cycle.

The CLTE values α were calculated at the two to five ranges of temperature as presented in Fig. 5, depending on the Ts of the material: $\Delta T_1 = 30$–45 ℃, $\Delta T_2 = 45$–60 ℃, $\Delta T_3 = 65$–100 ℃, $\Delta T_4 = 110$–140 ℃, $\Delta T_5 = 150$–165 ℃, as described in [23]

$$a_i = \frac{\Delta L_i}{L_0 \Delta T_i} \tag{1}$$

where ΔLi is the change of specimen length, L_0 is the initial length of the specimen, ΔTi is the temperature difference over which the change in material length was measured, $i = 1…5$ temperature difference over which the change in material length was measured.

The ITS was calculated from the displacement values measured at the first heating/cooling cycle (Fig. 4)

$$ITS = \frac{\Delta L}{L_0} \times 100\% \tag{2}$$

where $\Delta L = L_S - L_0$ is the change in length of the specimen between the first and second cycles, and L_S is the initial length of the specimen on the second cycle.

Fig. 4 Dependence of displacement and temperature as a function of time during TMA test for TPU95A sample
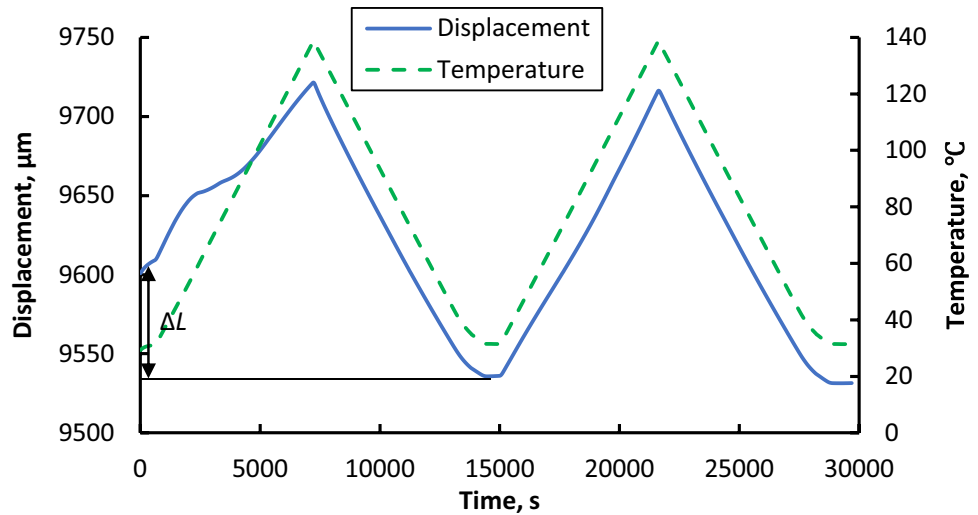
Fig. 5 Example of TMA (displacement vs temperature curve) for determination of CLTE at X-axis for PA
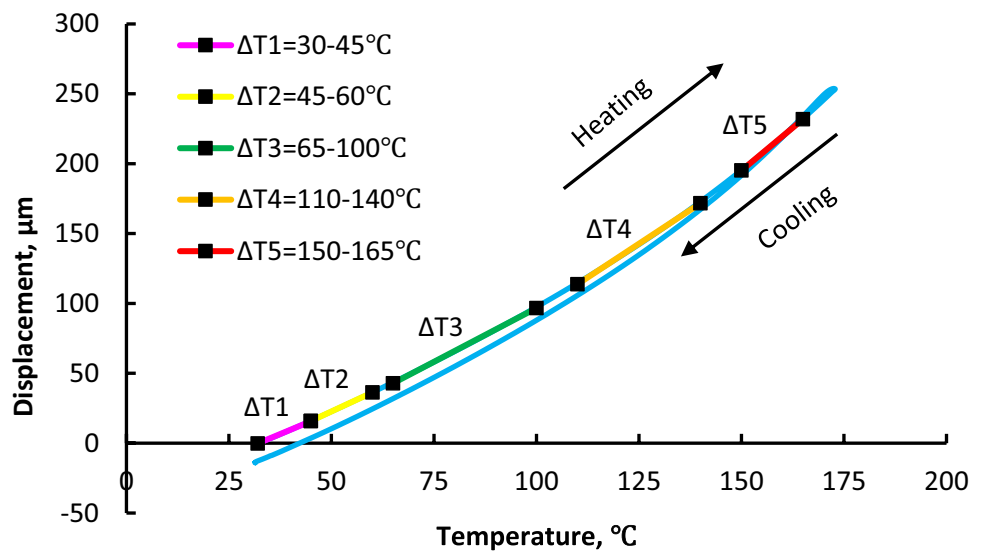
3.2 Thermal conductivity

Different methods can be used to characterise the thermal conductivity of 3D printed polymers, including the laser flash method [24], the transient plane source (TPS) method [9], and various steady-state techniques [19, 25–27]. The TPS method for anisotropic material requires materials with equal thermal conductivity in two directions, which is not the case for FDM printed samples. The original TPS method for the thermal conductivity and heat capacity measurements can be applied only to the isotropic and with some limitations to the transversely isotropic material. On the other side, the FDM-printed samples are generally anisotropic. A new method was developed for the identification of a three-dimensional thermal conductivity tensor using the TPS method combined with numerical simulations and inverse solution.

The samples' thermal conductivity and volumetric heat capacity were measured with Hot Disk TPS-500 equipment at room temperature. A two-sided configuration with a Kapton sensor 5465 of 3.189-mm radius was used.

Each pair of samples was tested at least three times with a heating power of 0.05–0.1 W and a measuring time of 40–80 s. The samples were removed from a measuring cell and reinstalled after each measurement with a cool-down period of at least 10 min.

The TPS tests were performed with the probe placed between two samples in three planes XY, XZ, and YZ. The experimental temperature curves were recorded and used later to calibrate the numerical model.

The finite element model of the transient heat conduction was used to simulate the heating of the sample in the TPS method for the thermal conductivity measurements. One-fourth of the sample was modelled using 3D
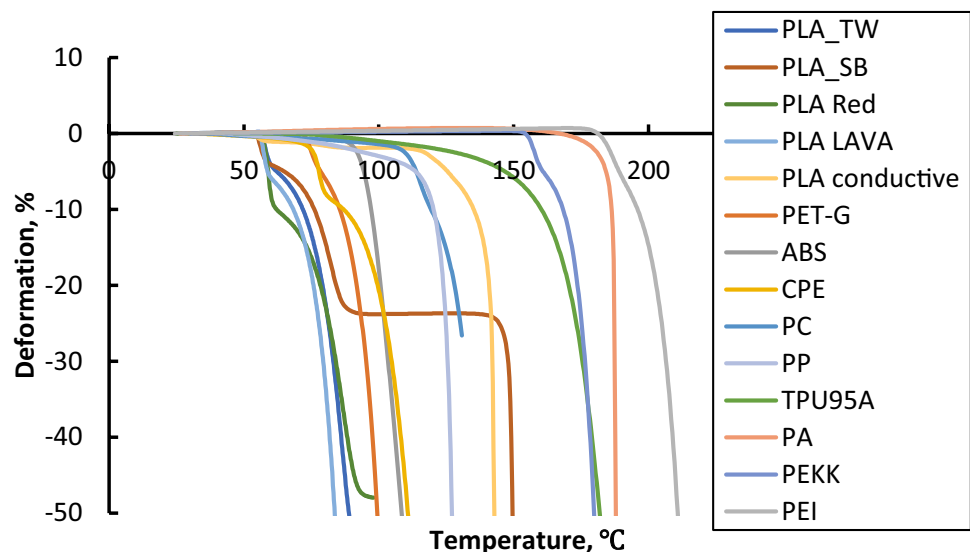
solid finite elements with the circular heat source/probe at the bottom of the sample. Constant heat generation in the probe was applied, and the heat dissipation in the sample was simulated in FE analysis. The average temperature of the probe was calculated at each time increment of the finite element solution and recorded for further processing.

To identify the unknown anisotropic thermal conductivity of the material, a multivariable optimisation procedure was implemented. The numerical temperature curves from simulations in three directions obtained in finite element solution were compared with experimental ones, and the root mean square error (RMSE) was calculated. A computer program implementing the Nelder-Mead optimisation algorithm was developed and used to find the best-fit anisotropic material parameters, allowing the identification of the material's thermal conductivity in principal directions K_x, K_y, and K_z.

3.3 Differential scanning calorimetry

Differential scanning calorimetry (DSC) measurements were conducted using a Mettler Toledo DSC 823e calorimeter. The weight of the tested samples was about 5 mg; aluminium crucibles with a pin were used for the test. The sample was kept at 25 ℃ for 5 min, then heated from 25 to 200 ℃ with subsequent cooling to 25 ℃ with a heating/cooling rate of 10 ℃/min. Samples were tested in nitrogen media. The samples were pieces of one 3D specimen, tested after a definite elapsed time t after the printing (storage time). Also, the reference specimen of PLA filament was tested. According to Mettler Toledo specification, temperature measuring accuracy was 0.2 K and for integral data $\pm 2\%$.

4 Results and discussion

4.1 Penetration

One of the study's objectives was to evaluate the upper limit of the operating temperatures of printed samples or the softening point. The penetration method was used for this purpose. TMA curves of the tested samples are presented in Fig. 6.

Figure 7 shows the distribution of T_S values by samples. As can be seen from the figure, PEI had the highest heat resistance of ca. $T_S = 185$ ℃. PLA samples had $T_S = 55$–57 ℃, which is the lowest of the studied products, except PLA conductive specimens filled with nanoparticles to provide electrical conductivity with a softening temperature of 138 ℃.

4.2 Coefficient of thermal expansion

With the help of TMA, the CLTE of the test samples was determined in three directions X, Y, and Z. The tests consisted of two heating/cooling cycles. A significant deformation was observed in the first cycle for almost all test samples, as shown in Fig. 4. Therefore, the CLTE values were determined in the second cycle, where the samples behaved more stably. CLTE values for all test materials for different temperature ranges and directions are presented in Table 2. As seen from the table, when comparing the first two temperature ranges (30–45 ℃ and 45–60 ℃), CLTE for most samples increases slightly, except for the samples of the PLA group. The CLTE values in all directions for most samples increased with increasing temperature range, and in some cases, these values increased sharply closer to the T_S.

Fig. 6 TMA curves of the deformation as a function of temperature for penetration of tested samples

Fig. 7 Softening temperature T_s of polymers identified by penetration
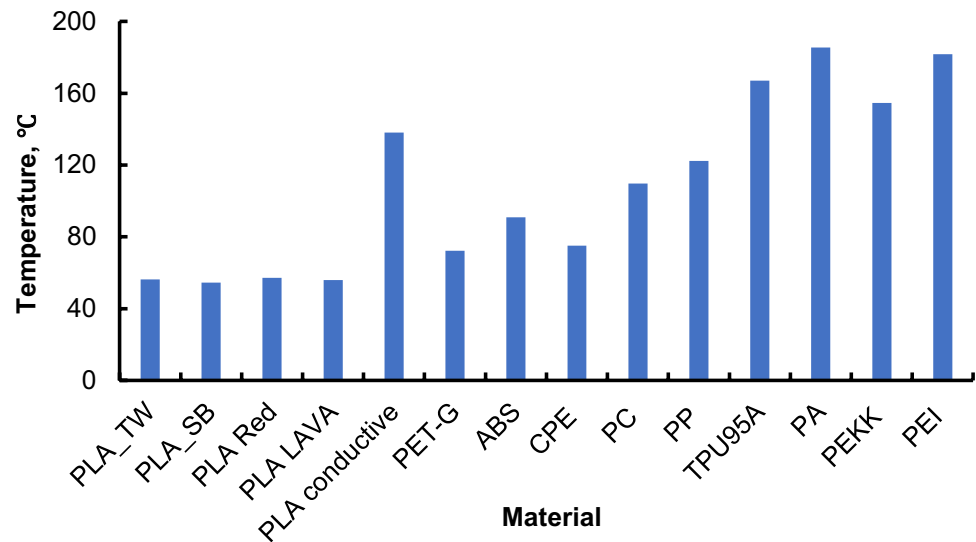
Materials such as PLA Conductive and TPU were thermally stable even at temperatures above 100 ℃; they did not show a significant increase in CLTE for all directions.

CLTE values of tested materials at a 30–45 ℃ range of the temperature are presented in diagram Fig. 8.

As can be seen from Fig. 8, PP and TPU have the highest thermal expansion coefficient of $\alpha \approx 2.0 \cdot 10^{-4}$ K^{-1}. The average estimated error for CLTE was about 10%. The large differences between the experimental and reference values of the CLTE can be explained by the fact that in the given study, the CLTE of the printed products was evaluated, but not the bulk material. The reference data are also difficult to compare because the conditions and methods for estimating the CLTE are not fully described.

In general, semi-crystalline polymers like PP, TPU95A, and PA have a higher CLTE than amorphous ones. Having values for CLTE in different directions, it seems possible to estimate the degree of anisotropy for a given property, defined as the ratio of two components of the same property in different directions. Some samples showed a pronounced anisotropic behaviour (PLA Red, PLA Conductive). In these cases, the degree of anisotropy is about 1.4. At a value close to 1, the behaviour of the material property is isotropic.

4.3 Irreversible thermal strain

The values of ITS calculated as described above for the tested samples are given in Table 3. When analysing the obtained data, it is essential to note that a large residual strain observed after the first heating/cooling cycle almost disappeared in the second cycle, as shown in Fig. 4. All samples shrunk in the print direction *X,* and most of them expanded in the build direction *Z*. TPU and PA demonstrated shrinkage in all three directions.

From the obtained data, PLA Red and CPE showed significant ITS of 9–10% and 6–7%, respectively, compared to samples from other materials, where ITS was 0.1–0.2%. Samples from materials such as PLA LAVA, ABS, PC, PP, and TPU demonstrated more stable thermal behaviour.

4.4 Thermal conductivity

Table 4 lists measured and numerically estimated properties of the studied samples: density, thermal conductivity in three orthogonal directions K_x, K_y, and K_z (with conductivity in the print direction designated as K_x, and conductivity in the build direction as K_z), and specific heat capacity C_p. An average of all measured values on three measurement planes (XY, XZ, and YZ) and the standard deviation is shown for specific heat in Table 4, showing good repeatability of the results. However, it should be noted that the uncertainty of the TPS method itself for the specific heat is about 10%. The uncertainty of the thermal conductivity values, identified through the inverse solution within an optimisation procedure, was estimated for similar samples made of ABS plastic, where thermal conductivity values could be reliably estimated using micromechanical analysis, and an agreement of about 10% was obtained for thermal conductivity values estimated by two different methods. The value of specific heat capacity for PLA Red measured by the TPS method is very close to $Cp = 1.33 \pm 0.03$ kJ/(kg·K) obtained by the direct measurement method from the DSC test.

The analysis of the obtained results shows that many specimens have a certain degree of anisotropy in thermal conductivity, defined as a ratio of a maximum and minimum principal thermal conductivity values of a sample. Practically isotropic conductivity was observed for some specimens, like ABS, PC, PLA LAVA, and PLA_TW. Detailed examination of these samples reveals the absence of voids

**Table 2** Values of CLTE (K^{-1}) at different ranges of temperature and directions

Material	ΔT, ℃				
	30–45	45–60	65–100	110–140	150–165
X					
PLA_TW	1.00E−04	2.17E−04	–	–	–
PLA Red	6.32E−05	1.12E−04	–	–	–
PLA_SB	9.16E−05	1.41E−04	–	–	–
PLA LAVA	9.27E−05	2.24E−04	–	–	–
PLA conductive	1.05E−04	1.27E−04	1.84E−04	1.76E−04	–
PET-G	7.21E−05	7.94E−05	1.43E−04	–	–
ABS	9.06E−05	9.78E−05	1.11E−04	–	–
CPE	6.95E−05	7.75E−05	−3.58E−05	–	–
PC	7.31E−05	7.60E−05	9.03E−05	–	–
PP	1.94E−04	2.25E−04	2.61E−04	–	–
TPU95A	1.69E−04	1.63E−04	1.66E−04	1.93E−04	
PA	1.26E−04	1.39E−04	1.58E−04	1.98E−04	2.51E−04
PEKK	4.63E−05	4.68E−05	4.88E−05	5.21E−05	1.16E−04
PEI	5.36E−05	5.28E−05	5.46E−05	5.98E−05	7.43E−05
Y					
PLA_TW	1.02E−04	2.28E−04	–	–	–
PLA Red	8.08E−05	1.15E−04	–	–	–
PLA_SB	9.11E−05	2.53E−04	–	–	–
PLA LAVA	9.30E−05	2.40E−04	–	–	–
PLA conductive	1.19E−04	1.45E−04	1.89E−04	1.66E−04	–
PET-G	7.26E−05	8.04E−05	1.92E−04	–	–
ABS	9.30E−05	1.01E−04	1.40E−04	–	–
CPE	7.76E−05	8.55E−05	2.60E−04	–	–
PC	7.35E−05	7.68E−05	9.15E−05	–	–
PP	2.00E−04	2.32E−04	2.68E−04	–	–
TPU95A	1.70E−04	1.73E−04	1.80E−04	1.99E−04	–
PA	1.20E−04	1.34E−04	1.51E−04	1.88E−04	2.37E−04
PEKK	4.58E−05	4.62E−05	4.82E−05	5.25E−05	1.64E−04
PEI	5.57E−05	5.52E−05	5.88E−05	6.60E−05	9.30E−05
Z					
PLA_TW	1.01E−04	2.07E−04	–	–	–
PLA Red	9.01E−05	1.27E−04	–	–	–
PLA_SB	9.50E−05	2.76E−04	–	–	–
PLA LAVA	9.46E−05	2.47E−04	–	–	–
PLA conductive	1.42E−04	1.73E−04	2.18E−04	1.75E−04	–
PET-G	7.40E−05	8.11E−05	2.40E−04	–	–
ABS	9.72E−05	1.04E−04	2.18E−04	–	–
CPE	6.94E−05	8.19E−05	4.50E−04	–	–
PC	7.91E−05	8.24E−05	1.02E−04	–	–
PP	2.16E−04	2.51E−04	2.88E-04	–	–
TPU95A	1.81E−04	1.76E−04	1.82E−04	2.08E−04	–
PA	1.17E−04	1.32E−04	1.49E−04	1.85E−04	2.37E−04
PEKK	4.68E−05	4.73E−05	4.89E−05	5.26E−05	1.65E−04
PEI	5.57E−05	5.79E−05	6.10E−05	6.83E−05	9.77E−05

(or very small voids) between extruded filaments. Samples with an anisotropy degree of about 1.3 and higher (e.g. PLA Red, PLA conductive, PEI, and PP) have a microstructure with voids elongated in the print direction, as shown in Fig. 9. Specimens were polished with a sand-paper up to 2000 grit and cleaned in an ultrasonic bath for about

Fig. 8 CLTE of tested samples at 30–45 ℃ range of the temperature and the reference values [28, 29]
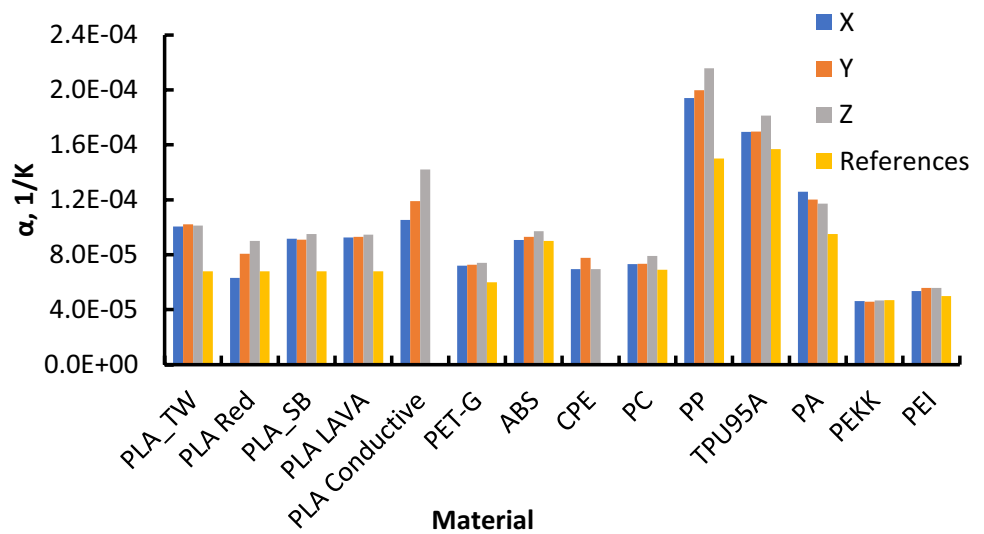
Table 3 Values of ITS (%) for tested materials at various directions

Material	Direction		
	X	**Y**	**Z**
PLA_TW	− 0.268	− 0.0936	0.712
PLA Red	− 9.13	− 0.240	9.95
PLA_SB	− 0.919	− 1.36	3.34
PLA LAVA	− 0.160	− 0.112	0.207
PLA Conductive	− 1.56	− 0.694	1.51
PET − G	− 1.24	− 0.170	0.676
ABS	− 0.0252	0.0969	0.0953
CPE	− 7.17	1.86	6.67
PC	− 0.246	− 0.134	0.287
PP	− 0.158	− 0.191	0.521
TPU95A	− 0.678	− 0.427	− 0.275
PA	− 0.884	− 0.961	− 0.522
PEKK	− 1.36	− 0.282	− 0.220
PEI	− 1.50	− 0.0831	0.278

Table 4 Physical properties of investigated samples

Material	Density, g/cm^3	K_x, W/m·K	K_y, W/m·K	K_z, W/m·K	C_p, kJ/kg·K
PLA_TW	1.227 ± 0.002	0.229	0.23	0.229	1.25 ± 0.08
PLA Red	1.203 ± 0.007	0.247	0.189	0.206	1.26 ± 0.04
PLA LAVA	1.246 ± 0.000	0.23	0.231	0.228	1.24 ± 0.06
PLA Conductive	1.212 ± 0.002	0.434	0.348	0.309	1.29 ± 0.13
PET-G	1.276 ± 0.003	0.248	0.23	0.246	1.12 ± 0.06
ABS	1.124 ± 0.001	0.228	0.223	0.227	1.26 ± 0.08
CPE	1.273 ± 0.002	0.271	0.252	0.235	1.09 ± 0.08
PC	1.191 ± 0.001	0.256	0.258	0.256	1.26 ± 0.11
PP	0.813 ± 0.016	0.286	0.181	0.178	1.96 ± 0.19
TPU95A	1.033 ± 0.019	0.246	0.253	0.187	1.78 ± 0.22
PA	1.103 ± 0.006	0.337	0.362	0.304	1.89 ± 0.09
PEKK	1.199 ± 0.003	0.242	0.235	0.241	1.06 ± 0.07
PEI	1.173 ± 0.001	0.269	0.191	0.183	1.12 ± 0.10

5–10 min. The samples made from white or semi-transparent polymers were also polished with "GOI" paste to fill in the pores with dark paste for better contrast.

As the thermal properties of FDM printed samples may be affected by printer settings [20, 21], direct comparison with other published results is not always possible. However, good agreement was found for the conductivity of the ABS [30], TPU [31], PLA, and PLA conductive [20] samples.

For materials with a pronounced degree of anisotropy, the highest value of thermal conductivity usually was obtained for print direction, as could be expected [19, 20], except for PA samples, where the highest conductivity was obtained in the *Y* direction.

Micromechanical finite element analysis of a representative volume element with voids similar to the ones presented in Fig. 9 showed that the voids alone could not lead to high anisotropy in the thermal properties. Thermal contact resistance between adjacent extruded filaments is a possible source of significant anisotropy in the measured thermal conductivities [25].

4.5 Post-printing relaxation of a structure

3D printing of many plastics is usually accompanied by rapid cooling to prevent the layers from changing shape after printing. The temperature difference during the printing of the sample between the area at the extruder nozzle and the area printed a few minutes earlier, referred to as the elapsed time, allowed us to get this estimate of the cooling rate from the moment of melting. Samples produced by such

Fig. 9 Microstructure of 3D printed samples at a plane perpendicular to *X*-axis: PLA Red (**a**), PLA conductive (**b**), PEI (**c**), and PP (**d**)
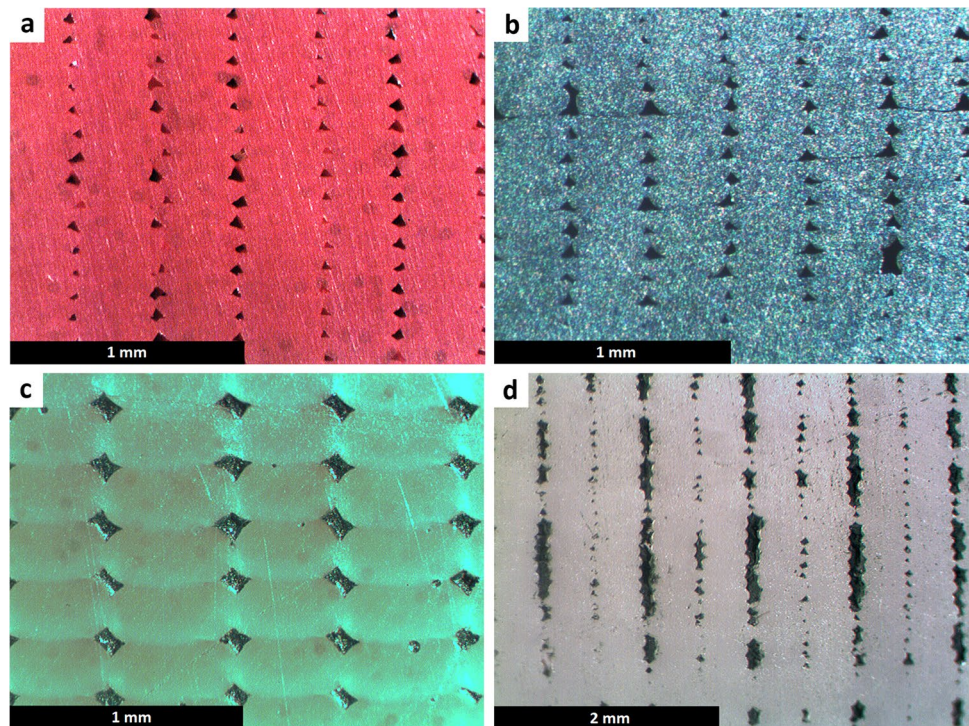
3D printing from semi-crystalline PLA material usually have a non-equilibrium structure with a low degree of crystallinity. Such structures may change in time after printing, which affects the stiffness and strength of the printed samples. Also, they may noticeably differ from the structure of the original filament used. The filament was manufactured more than six months ago and kept for this time under normal conditions.

This part of the work aimed to reveal the changes in PLA samples' structure during storage by DSC measurements. Corresponding tasks of the work are:

- Selection of characteristic temperatures and enthalpies associated with the samples' structure changes.
- Experimental evaluation of the structural changes during storage with DSC measurements.
- Comparison of the structural changes with changes in the mechanical properties during storage.

Only the first heating cycle was studied in the experiments to avoid distorting the history of heat treatment of printed samples. A typical PLA thermogram contains a glass transition with temperature T_g corresponding to the inflexion point after the initial flat heat flow. The transition is accompanied by a small endothermic peak typifying the enthalpy relaxation phenomenon [32] with temperature extrapolated to T_{Hr} (Fig. 10). In this phenomenon, the temperature and mobility of polymer chains are sufficient for their recovery to a thermodynamic equilibrium state.

Enthalpy relaxation could be affected by the specimens' crystallinity state and thermal history [33]. The thermal parameters from DSC thermograms are shown in Table 5.

The cold crystallisation exothermic peak with $T_{cc} \approx$ 112 °C occurs while heating above the glass transition temperature. The associated enthalpy change is denoted $\Delta H_{cc} \approx -23$ J/g for the printed PLA sample. The value is noticeably lower $\Delta H_{cc} = -18$ J/g for the reference filament sample.

The cold crystallisation peak is immediately followed by the endothermic melting peak with a temperature $T_m \approx$ 150 °C. When cooling from ca. 200 °C at 10 ℃/min, the PLA sample hardly crystallises, and a barely visible exothermic peak at flat heat flow is noticeable in the cooling part of the thermogram (Fig. 10). All thermal changes of the PLA and the main values obtained during the DSC measurements are in accordance with the results [33–45].

Analysing the results of DSC measurements presented in Table 5, one can see that values of T_g and T_{Hr} of the reference specimen of original PLA filament differ noticeably from that of 3D printed samples. Figure 11 and Fig. 12 illustrate the difference mentioned and the instability of these values during the first 200 h of storage, but with values lower than the original filament. With an increase of storage duration over 200 h, there was a tendency for stabilisation of the mentioned values while still being below that of the original filament. This fact means that the PLA structure changes noticeably during 3D printing and does not return to the initial properties of the filament.

Fig. 10 Heat flow (mW) vs temperature (°C) for 3D printed specimens in DSC test: Fresh sample (black line) with storage time less than 1 day; old sample (red line) with storage time more than 16 days
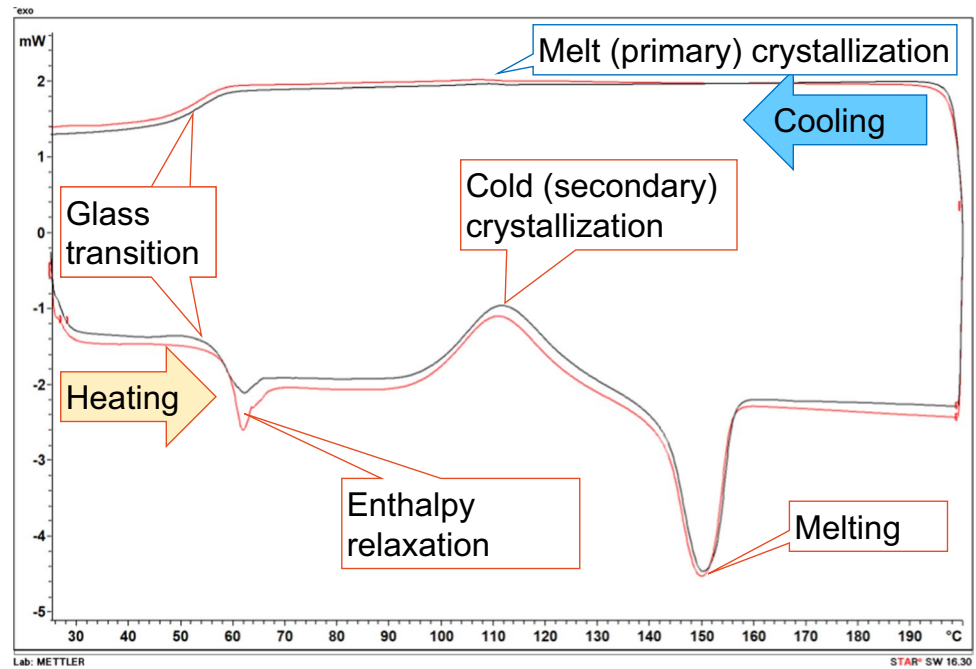
Table 5 Thermal properties of the 3D printed PLA specimens depending on the storage time

t, h	Glass Transition, heating		Cold crystallisation (recrystal-lisation)		Melting	Degree of crystallinity
	T_g, °C	T_{Hr}, °C	T_{cc}, °C	ΔH_{cc}, J/g	T_m, °C	χ_c, %
0*	60.22	64.04	111.33	− 18.42	150.67	4.66
2	58.31	61.24	112.00	− 25.27	150.17	1.48
27	57.82	60.73	112.17	− 22.14	149.83	0.34
51	57.72	61.24	112.17	− 24.43	149.50	2.02
97	57.52	59.93	110.67	− 20.40	148.50	2.46
166	58.65	61.06	112.83	− 24.94	150.17	2.98
358	58.59	61.33	111.33	− 22.08	149.00	1.19
600	58.97	61.73	110.83	− 24.64	150.00	2.60

*The original 3D printing filament was stored for 6 months under normal conditions.

In semi-crystalline PLA, the structure changes could be mainly connected to the crystallisation process. Changes of enthalpy during cold crystallisation ΔH_{cc} are greater for 3D printed specimens (see Table 5). That can be related to the lower degree of crystallinity χ_c of the printed PLA samples, which was calculated as in [33]

$$X_c = \frac{|\Delta H_m + \Delta H_{cc}|}{\Delta H^*}100\%$$

where ΔH_m is the enthalpy change associated with the endothermic melting peak (positive value) and ΔH^* is the melting enthalpy of the pure PLA crystal equal to 93 J/g [33].

The degree of crystallinity χ_c during heating of the original filament and 3D printed specimen depending on storage time t (Fig. 13) also demonstrates instability during 400-h storage with lower values than that of the original filament.

Elastic modulus and extruded fibre strength, depending on storage time, are presented in Fig. 14. As seen from the figure, the modulus and strength of a fibre initially exhibit a steady increase in time and stabilisation after approximately 200–300 h [46]. The average modulus of $E = 3.57 \pm 0.11$ GPa over a time interval was chosen as Young's modulus of printed material.

The results of DSC measurements and tensile tests allow concluding that when the routine 3D printing process is accompanied by rapid cooling, the PLA sample hardly crystallises. This confirms by a barely visible exothermic peak — primary crystallisation at flat heat flow in the thermogram when cooling at 10 °C/min (see Fig. 10).

Fig. 11 Glass transition temperature T_g of original filament and 3D printed specimen after different storage time t
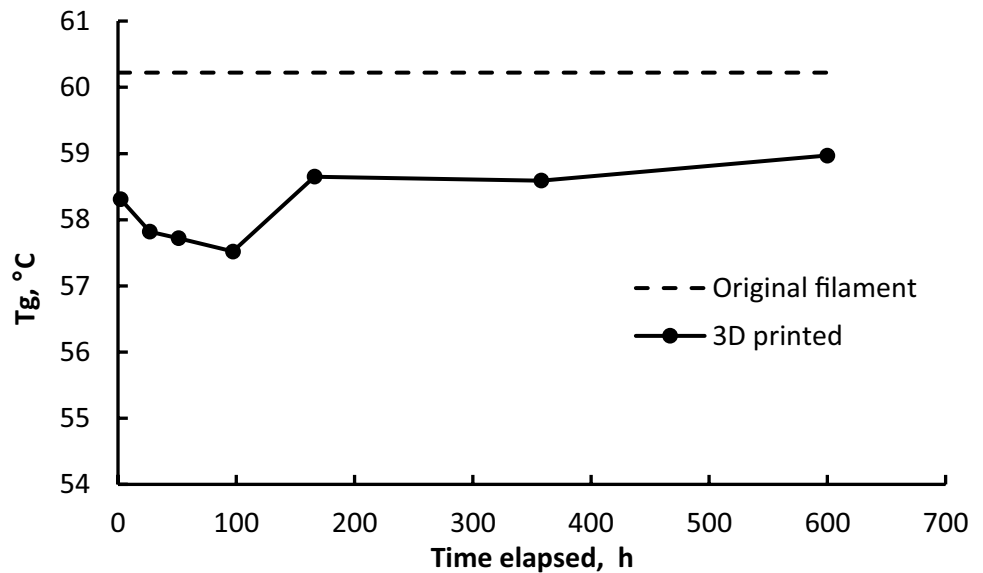
Fig. 12 The extrapolated peak of enthalpy relaxation T_{Hr} of original filament and 3D printed specimen after different storage time t
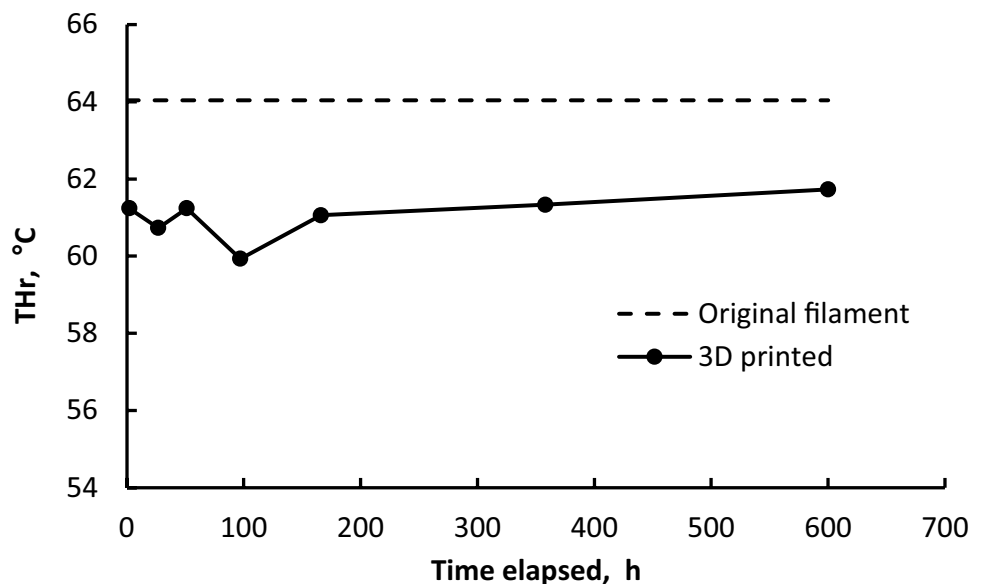
The low degree of crystallinity reduces the mechanical characteristics of 3D printed samples.

The phenomenon of cold crystallisation and recrystallisation in the interval of 100–130 °C is associated with noticeable enthalpy changes that allow annealing 3D printed PLA samples and increase the crystallinity of products. Experiments on short-term (from 10 min to 1 h) annealing of the printed samples at the temperature mentioned and their DSC tests confirmed the assumption about the increase in the degree of crystallinity. On the thermograms of the annealed samples, the exothermic peak of primary crystallisation completely disappeared, while the endothermic melting peak at ca. 150 °C was retained. The calculated degree of crystallinity χ_c increased up to 30–40%, approaching and reaching

the upper limit of this degree (40%) for semi-crystalline PLA [47].

The results obtained allow us to recommend the annealing of finished 3D printed PLA parts to improve their mechanical properties (stiffness and strength) by increasing the degree of crystallinity of the material [48, 49].

5 Conclusions

The purpose of this study was to evaluate, systematise, and provide a comparative analysis of the main thermal characteristics of 3D printed samples from the most common thermoplastic materials.

Fig. 13 Degree of crystallinity χ_c during heating of original filament and 3D printed specimen depending on storage time t
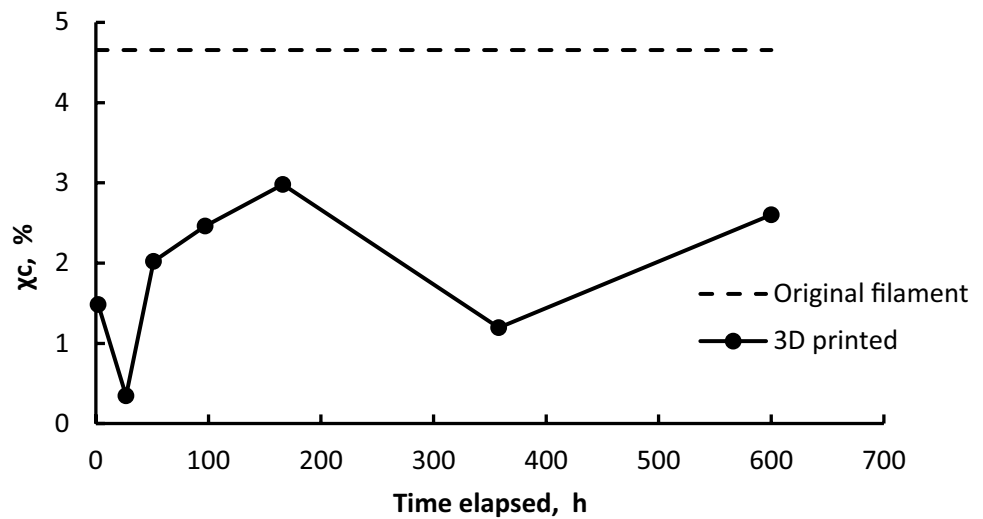
Fig. 14 Change of elastic modulus and strength of a single PLA fibre with time after extrusion [46]
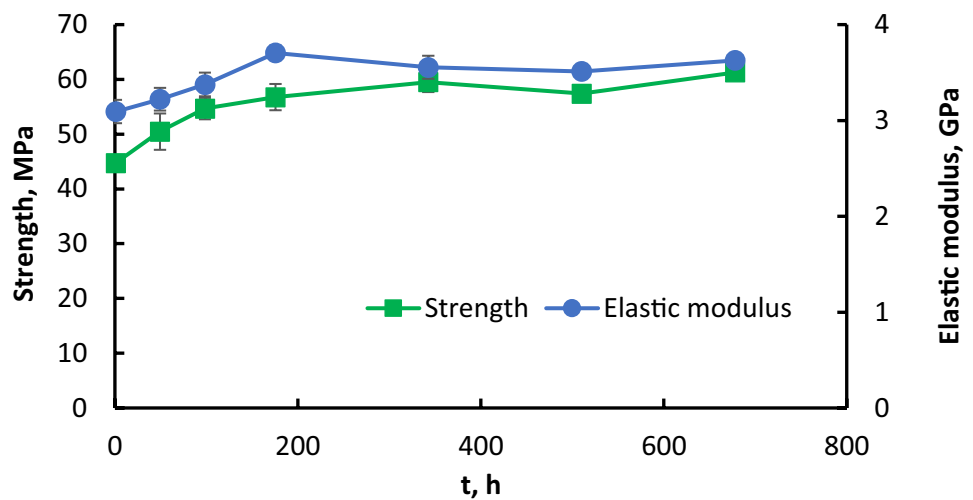
During the work, the softening temperature of the 3D printing products was determined. CLTE, ITS, thermal conductivity, heat capacity, and post-printing relaxation of a structure of the 3D-printing samples were evaluated in the various directions of the measurements for a broad range of typical materials used in FDM printing.

The main results of the study were:

1. The upper limit of the operating temperature range for 3D printed samples was determined – the softening temperature T_S. The most thermally stable samples were PA with ca. $T_S = 185$ ℃, while the PLA samples with $T_S = 55$–57 ℃ were the least thermally stable.

2. Significant irreversible thermal strain (ITS) was observed in the first heating cycle in almost all the samples under the study, and it almost disappeared in the second cycle.

3. The values of the CLTE at different temperature ranges in all three measurement directions were estimated in the second cycle. All tested products shrunk in the print direction X, and nearly all expanded in the build direction Z.

4. The thermal conductivity was measured in three orthogonal directions along the principal axes of the printed unidirectional samples. The highest degree of anisotropy of CLTE, about 1.35–1.42, was seen for PLA RED and PLA Conductive samples. The highest degree of thermal conductivity anisotropy, 1.4–1.6, was observed for PP and PLA conductive samples. The results showed almost isotropic behaviour for some samples, e.g. PLA_TW, and PLA LAVA, and some degree of anisotropy in conductive properties for other samples.

5. During the first heating cycle, the glass transition temperature and the degree of crystallinity showed instabil-

ity of their values during storage but with values lower than those of the original filament material. With an increase in the duration of storage over 200–400 h, there was a tendency to stabilise the indicated values. Similar behaviour was observed for the modulus and strength values of the 3D printed single PLA fibre during storage. The PLA sample hardly crystallises when rapidly cooling after 3D printing.

6. The ITS phenomenon during primary heating can be critical for some products. It is recommended to do primary annealing of 3D printed products to T_S to improve the structural stability of PLA samples by increasing the degree of crystallinity.

The analysis of the influence of the size and shape of the pores on the thermal conductivity anisotropy of different samples, and the existence and characterisation of the thermal contact resistance between extruded filaments in these samples, requires more detailed study and additional tests with different printing settings for each material.

Author contribution Irina Bite: conceptualisation, formal analysis, writing—original draft, writing—review & editing.

Sergejs Tarasovs: conceptualisation, methodology, software, formal analysis, writing—original draft, writing—review & editing.

Sergejs Vidinejevs: conceptualisation, formal analysis, writing—original draft, writing—review & editing.

Laima Vevere: investigation.

Jevgenijs Sevcenko: investigation.

Andrey Aniskevich: conceptualisation, writing—review & editing, supervision, funding acquisition.

Declarations

Competing interests The authors declare no competing interests.

References

1. ISO/ASTM 52900 (2015) Standard terminology for additive manufacturing – general principles – terminology. ASTM International, West Conshohocken, PA

2. Bozkurt Y, Karayel E (2021) 3D printing technology; methods, biomedical applications, future opportunities and trends. J Mat Res and Tech 14:1430–1450. https://doi.org/10.1016/j.jmrt.2021.07.050

3. Buchanan C, Gardner L (2019) Metal 3D printing in construction: a review of methods, research, applications, opportunities and challenges. Eng Struct 180:332–348. https://doi.org/10.1016/j.engstruct.2018.11.045

4. Curran S, Chambon P, Lind R, Love L, Wagner R, Whitted S et al (2016) Big area additive manufacturing and hardware-in-the-loop for rapid vehicle powertrain prototyping: a case study on the development of a 3-D-printed Shelby cobra. SAE Tech Papers 0328. https://doi.org/10.4271/2016-01-0328

5. Zadpoor A, Malda J (2016) Additive manufacturing of biomaterials, tissues, and organs. Ann Biomed Eng 45:1–11. https://doi.org/10.1007/s10439-016-1719-y

6. Kristiawan R, Imaduddin F, Ariawan D, Sabino U, Arifin Z (2021) A review on the fused deposition modeling (FDM) 3D printing: filament processing, materials, and printing parameters. Open Eng 11:639–649. https://doi.org/10.1515/eng-2021-0063

7. Ngo TD, Kashani A, Imbalzano G, Nguyen KTQ, Hui D (2018) Additive manufacturing (3D printing): a review of materials, methods, applications and challenges. Composites Part B: Eng 143:172–196. https://doi.org/10.1016/j.compositesb.2018.02.012

8. Trhlíková L, Zmeskal O, Psencik P, Florian P (2016) Study of the thermal properties of filaments for 3D printing. AIP Conf Proc 1752(1):040027. https://doi.org/10.1063/1.4955258

9. Shemelya C, De La Rosa A, Torrado AR, Yu K, Domanowski J, Bonacuse PJ et al (2017) Anisotropy of thermal conductivity in 3D printed polymer matrix composites for space based cube satellites. Addit Manuf 16:186–196. https://doi.org/10.1016/j.addma.2017.05.012

10. Zhang W, Wu AS, Sun J, Quan Z, Gu B, Sun B et al (2017) Characterization of residual stress and deformation in additively manufactured ABS polymer and composite specimens. Composites Sci Technol 150:102–110. https://doi.org/10.1016/j.compscitech.2017.07.017

11. D'Amico A, Debaie A, Peterson A (2017) Effect of layer thickness on irreversible thermal expansion and interlayer strength in fused deposition modeling. Rapid Prototyp 23:00–00. https://doi.org/10.1108/RPJ-05-2016-0077

12. Agag T, Koga T, Takeichi T (2001) Studies on thermal and mechanical properties of polyimide–clay nanocomposites. Polymer 42(8):3399–3408. https://doi.org/10.1016/S0032-3861(00)00824-7

13. D'Amico T, Barrett C, Presing J, Peterson AM (2019) Micromechanical modeling of irreversible thermal strain. Addit Manuf 27:91–98. https://doi.org/10.1016/j.addma.2019.02.019

14. Zohdi N, Yang R (2021) Material anisotropy in additively manufactured polymers and polymer composites: a review. Polymers 13(19):3368. https://doi.org/10.3390/polym13193368

15. Spoerk M, Savandaiah C, Arbeiter F, Traxler G, Cardon L, Holzer C et al (2018) Anisotropic properties of oriented short carbon fibre filled polypropylene parts fabricated by extrusion-based additive manufacturing. Composites Part A: App Sci Manuf 113:95–104. https://doi.org/10.1016/j.compositesa.2018.06.018

16. Ibrahim Y, Elkholy A, Schofield JS, Melenka GW, Kempers R (2020) Effective thermal conductivity of 3D-printed continuous fiber polymer composites. Adv Manuf: Polym Comp Sci 6(1):17–28. https://doi.org/10.1080/20550340.2019.1710023

17. Luo F, Yang S, Yan P, Li H, Huang B, Qian Q et al (2022) Orientation behavior and thermal conductivity of liquid crystal polymer composites based on three-dimensional printing. Composites Part A: App Sci and Manuf 160:107059. https://doi.org/10.1016/j.compositesa.2022.107059

18. Hassen AA, Dinwiddie RB, Kim S, Tekinalp HL, Kumar V, Lindahl J et al (2022) Anisotropic thermal behavior of extrusion-based large scale additively manufactured carbon-fiber reinforced thermoplastic structures. Polym Compos 43(6):3678–3690. https://doi.org/10.1002/pc.26645

19. Elkholy A, Kempers R (2022) An accurate steady-state approach for characterizing the thermal conductivity of Additively manufactured polymer composites. Case Stud Therm Eng 31:101829. https://doi.org/10.1016/j.csite.2022.101829

20. Elkholy A, Rouby M, Kempers R (2019) Characterization of the anisotropic thermal conductivity of additively manufactured

components by fused filament fabrication. Prog in Addit Manuf 4(4):497–515. https://doi.org/10.1007/s40964-019-00098-2

21. Ravoori D, Alba L, Prajapati H, Jain A (2018) Investigation of process-structure-property relationships in polymer extrusion based additive manufacturing through in situ high speed imaging and thermal conductivity measurements. Addit Manuf 23:132–139. https://doi.org/10.1016/j.addma.2018.07.011

22. Prajapati H, Chalise D, Ravoori D, Taylor RM, Jain A (2019) Improvement in build-direction thermal conductivity in extrusion-based polymer additive manufacturing through thermal annealing. Addit Manuf 26:242–249. https://doi.org/10.1016/j.addma.2019.01.004

23. ASTM E831-06 (2021) Standard test method for linear thermal expansion of solid materials by thermomechanical analysis. ASTM International, West Conshohocken, PA. https://doi.org/10.1520/E0831-06

24. Guo R, Ren Z, Bi H, Xu M, Cai L (2019) Electrical and Thermal Conductivity of Polylactic Acid (PLA)-Based Biocomposites by incorporation of nano-graphite fabricated with fused deposition modeling. Polymers 11:549. https://doi.org/10.3390/polym11030549

25. Prajapati H, Ravoori D, Woods R (2018) Measurement of anisotropic thermal conductivity and inter-layer thermal contact resistance in polymer fused deposition modeling (FDM). Addit Manuf 21:84–90. https://doi.org/10.1016/j.addma.2018.02.019

26. Flaata T, Michna GJ, Letcher T (2017) Thermal conductivity testing apparatus for 3D printed materials. ASME 2017 Heat Transfer Summer Conference, p V002T15A006. https://doi.org/10.1115/HT2017-4856

27. Laureto J, Tomasi J, King J, Pearce J (2017) Thermal properties of 3-D printed polylactic acid-metal composites. Prog in Addit Manuf 2(1):57–71. https://doi.org/10.1007/s40964-017-0019-x

28. Filament Properties Table. https://www.simplify3d.com/support/materials-guide/properties-table/. Accessed 20 Apr 2022

29. Coefficient of Linear Thermal Expansion. https://omnexus.specialchem.com/polymer-properties/properties/coefficient-of-linear-thermal-expansion. Accessed 21 Apr 2022

30. Sonsalla T, Moore AL, Meng WJ, Radadia AD, Weiss L (2018) 3-D printer settings effects on the thermal conductivity of acrylonitrile butadiene styrene (ABS). Polym Test 70:389–395. https://doi.org/10.1016/j.polymertesting.2018.07.018

31. Liu J, Li W, Guo Y, Zhang H, Zhang Z (2019) Improved thermal conductivity of thermoplastic polyurethane via aligned boron nitride platelets assisted by 3D printing. Compos Part A: App Sci Manuf 120:140–146. https://doi.org/10.1016/j.compositesa.2019.02.026

32 Hodge IM, Berens AR (1982) Effects of annealing and prior history on enthalpy relaxation in glassy polymers. 2. Mathematical modeling. Macromol 15(3):762–770. https://doi.org/10.1021/ma00231a016

33. Yu W, Wang X, Ferraris E, Zhang J (2019) Melt crystallization of PLA/Talc in fused filament fabrication. Mat Des 182:108013. https://doi.org/10.1016/j.matdes.2019.108013

34. Tábi T, Sajó I, Szabó F, Luyt A, Kovács J (2010) Crystalline structure of annealed polylactic acid and its relation to processing. Express Polym Lett 4(10):659–668. https://doi.org/10.3144/expresspolymlett.2010.80

35. Mróz P, Białas S, Mucha M, Kaczmarek H (2013) Thermogravimetric and DSC testing of poly(lactic acid) nanocomposites. Thermochim Acta 573:186–192. https://doi.org/10.1016/j.tca.2013.09.012

36. Gordobil O, Egüés I, Llano-Ponte R, Labidi J (2014) Physicochemical properties of PLA lignin blends. Polym Degrad Stab 108:330–338. https://doi.org/10.1016/j.polymdegradstab.2014.01.002

37. Harris AM, Lee EC (2008) Improving mechanical performance of injection molded PLA by controlling crystallinity. J Appl Polym Sci 107(4):2246–2255. https://doi.org/10.1002/app.27261

38. Kaczmarek H, Nowicki M, Vuković-Kwiatkowska I, Nowakowska S (2013) Crosslinked blends of poly(lactic acid) and polyacrylates: AFM, DSC and XRD studies. J Polym Res 20(3):91. https://doi.org/10.1007/s10965-013-0091-y

39. Day M, Nawaby A, Liao X (2006) A DSC study of the crystallization behaviour of polylactic acid and its nanocomposites. J Therm Anal Calorim 86(3):623–629. https://doi.org/10.1007/s10973-006-7717-9

40. García NL, Lamanna M, D'Accorso N, Dufresne A, Aranguren M, Goyanes S (2012) Biodegradable materials from grafting of modified PLA onto starch nanocrystals. Polym Degrad Stab 97(10):2021–2026. https://doi.org/10.1016/j.polymdegradstab.2012.03.032

41. Drummer D, Cifuentes-Cuéllar S, Rietzel D (2012) Suitability of PLA/TCP for fused deposition modeling. Rapid Prototyp 18(6):500–507. https://doi.org/10.1108/13552541211272045

42. Wootthikanokkhan J, Cheachun T, Sombatsompop N, Thumsorn S, Kaabbuathong N, Wongta N et al (2013) Crystallization and thermomechanical properties of PLA composites: Effects of additive types and heat treatment. J Appl Polym Sci 129(1):215–223. https://doi.org/10.1002/app.38715

43. Fu ZJ, Huang HF, Yu LS, Sun YF (2013) DSC studies on the dyeing properties of PLA fiber. Adv Mat Res 750–752:1393–1396. https://doi.org/10.4028/www.scientific.net/AMR.750-752.1393

44. Běhálek L, Maršálková M, Lenfeld P, Habr J, Bobek J, Seidl M (2013) Study of crystallization of polylactic acid composites and nanocomposites with natural fibres by DSC method. NANOCON 2013 - Conference Proceedings, 5th International Conference pp 746–751

45. Cao X, Mohamed A, Gordon S, Willett J, Sessa D (2003) DSC study of biodegradable poly (lactic acid) and poly (hydroxy ester ether) blends. Thermochim Acta 406(1–2):115–127. https://doi.org/10.1016/S0040-6031(03)00252-1

46. Zile E, Zeleniakiene D, Aniskevich A (2022) Characterization of polylactic acid parts produced using fused deposition modelling. Mech Compos Mater 58(2):169–180. https://doi.org/10.1007/s11029-022-10021-6

47. Pan P, Zhu B, Kai W, Dong T, Inoue Y (2008) Polymorphic transition in disordered poly(l-lactide) crystals induced by annealing at elevated temperatures. Macromol 41(12):4296–4304. https://doi.org/10.1021/ma800343g

48. Dusunceli N, Colak OU (2008) Modelling effects of degree of crystallinity on mechanical behavior of semicrystalline polymers. Int J Plast 24(7):1224–1242. https://doi.org/10.1016/j.ijplas.2007.09.003

49. Lona Batista N, Olivier P, Bernhart G, Rezende Cerqueira M, Botelho Cocchieri E (2016) Correlation between degree of crystallinity, morphology and mechanical properties of PPS/carbon fiber laminates. Mat Res 19(1):195–201. https://doi.org/10.1590/1980-5373-MR-2015-0453